Allergy Asthma Immunol Res. 2020 Mar;12(2):306-321
https://doi.org/10.4168/aair.2020.12.2.306
pISSN 2092-7355·eISSN 2092-7363

Allergy, Asthma & Immunology Research AAIR

Original Article

Check for updates

Evaluation of Neo-Osteogenesis in Eosinophilic Chronic Rhinosinusitis Using a Nasal Polyp Murine Model

Roza Khalmuratova,[1†] **Mingyu Lee**,[1,2,3†] **Jong-Wan Park**,[1,2,3,4] **Hyun-Woo Shin**[1,2,3,4,5*]

[1]Obstructive Upper airway Research (OUaR) Laboratory, Department of Pharmacology, Seoul National University College of Medicine, Seoul, Korea
[2]Department of Biomedical Sciences, Seoul National University College of Medicine, Seoul, Korea
[3]Cancer Research Institute, Seoul National University College of Medicine, Seoul, Korea
[4]Ischemic/Hypoxic Disease Institute, Seoul National University College of Medicine, Seoul, Korea
[5]Department of Otorhinolaryngology-Head and Neck Surgery, Seoul National University Hospital, Seoul, Korea

OPEN ACCESS

Received: Sep 11, 2019
Accepted: Oct 19, 2019

Correspondence to
Hyun-Woo Shin, MD, PhD
Department of Pharmacology, Seoul National University College of Medicine, 103 Daehak-ro, Jongno-gu, Seoul 03080, Korea.
Tel: +82-2-740-8285
Fax: +82-2-745-7996
E-mail: charlie@snu.ac.kr

†Roza Khalmuratova and Mingyu Lee contributed equally to this manuscript.

Copyright © 2020 The Korean Academy of Asthma, Allergy and Clinical Immunology · The Korean Academy of Pediatric Allergy and Respiratory Disease
This is an Open Access article distributed under the terms of the Creative Commons Attribution Non-Commercial License (https://creativecommons.org/licenses/by-nc/4.0/) which permits unrestricted non-commercial use, distribution, and reproduction in any medium, provided the original work is properly cited.

ORCID iDs
Roza Khalmuratova
https://orcid.org/0000-0002-8518-4034
Mingyu Lee
https://orcid.org/0000-0002-8970-1895
Jong-Wan Park
https://orcid.org/0000-0003-4676-5191
Hyun-Woo Shin
https://orcid.org/0000-0002-4038-9992

ABSTRACT

Purpose: Osteitis refers to the development of new bone formation and remodeling of bone in chronic rhinosinusitis (CRS) patients; it is typically associated with eosinophilia, nasal polyps (NPs), and recalcitrant CRS. However, the roles of ossification in CRS with or without NPs remain unclear due to the lack of appropriate animal models. Thus, it is necessary to have a suitable animal model for greater advances in the understanding of CRS pathogenesis.
Methods: BALB/c mice were administered ovalbumin (OVA) and staphylococcal enterotoxin B (SEB). The numbers of osteoclasts and osteoblasts and bony changes were assessed. Micro computed tomography (micro-CT) scans were conducted to measure bone thickness. Immunofluorescence, immunohistochemistry, and quantitative polymerase chain reaction were performed to evaluate runt-related transcription factor 2 (RUNX2), osteonectin, interleukin (IL)-13, and RUNX2 downstream gene expression. Gene set enrichment analysis was performed in mucosal tissues from control and CRS patients. The effect of resveratrol was evaluated in terms of osteogenesis in a murine eosinophilic CRS NP model.
Results: The histopathologic changes showed markedly thickened bones with significant increase in osteoblast numbers in OVA/SEB-treated mice compared to the phosphate-buffered saline-treated mice. The structural changes in bone on micro-CT were consistent with the histopathological features. The expression of RUNX2 and IL-13 was increased by the administration of OVA/SEB and showed a positive correlation. RUNX2 expression mainly co-localized with osteoblasts. Bioinformatic analysis using human CRS transcriptome revealed that IL-13-induced bony changes via RUNX2. Treatment with resveratrol, a candidate drug against osteitis, diminished the expression of IL-13 and RUNX2, and the number of osteoblasts in OVA/SEB-treated mice.
Conclusions: In the present study, we found the histopathological and radiographic evidence of osteogenesis using a previously established murine eosinophilic CRS NP model. This animal model could provide new insights into the pathophysiology of neo-osteogenesis and provide a basis for developing new therapeutics.

Keywords: Chronic; sinusitis; nose; nasal polyps; eosinophilia; osteogenesis; IL-13; RUNX2 protein; mouse; animal models

Generated by xmlinkpress

Disclosure

There are no financial or other issues that might lead to conflict of interest.

INTRODUCTION

Chronic rhinosinusitis (CRS) is one of the most prevalent chronic diseases in humans; it affects up to 12.5% of the US population and has a significant socioeconomic impact.[1,2] CRS is mainly characterized by inflammatory disease of the paranasal sinuses and mucosa of the nose.[3,4] Among the various pathophysiological processes of CRS, association of osteitis has been reported as part of CRS development and maintenance.[3] Osteitis is a process of neo-osteogenesis and remodeling of the bone in CRS patients.[5] Previous studies have demonstrated the close contact between nasal mucosa and paranasal bones in patients with CRS using radiological methods, suggesting the contribution of this tissue toward favoring bone remodeling.[6,7] Also, association of ethmoid bone in osteitis has previously been demonstrated.[8]

A previous study reported that 36% of primary CRS patients showed evidence of new bone formation.[9] In addition, several studies revealed that bone inflammation in patients with CRS varies from 36% to 100%.[10] In particular, the osteitic bone acts as a nidus for inflammation, possibly contributing to the recurrence of CRS after surgical treatment.[11] Various studies indicate that osteitis positively correlates with poor prognosis of endoscopic sinus surgery and recalcitrant CRS.[12,13] Moreover, osteitis is associated with worse computed tomography (CT) outcomes, tissue eosinophilia, nasal polyps (NPs), and serum eosinophilia.[14-16] Although it is necessary to understand the involvement of osteitis in terms of CRS progression, the mechanisms underlying regulation of bony changes in chronic inflammatory conditions are poorly understood due to the lack of appropriate animal models, making clinical and experimental studies difficult.

Until now, rabbits have been used as experimental animal models for studying osteitis in CRS, and these studies showed inflammatory participation of the underlying bone matrix and the Haversian system. [7,17-21] The observations, including mucosal inflammation and signs of new or re-modeled bones in rabbits, support the idea that bone formation could participate in CRS progression. However, considering that bacteria in the bones of the paranasal sinuses have never been described, most of the recent studies using animal models with bacteria inoculation into the maxillary sinuses of rabbit are not comparable disease models to human CRS. Certain areas in the nasal sinus were also injured during the inoculation process, and this could induce tissue inflammation regardless of infection. In addition, the rabbit osteitis model has disadvantages in terms of higher housing cost and unavailability of genetic manipulation. Therefore, establishing a proper murine model for neo-osteogenesis facilitates the study of the roles of osteitis in greater depth, and this may improve the development of novel therapeutic agents to treat refractory osteitis in CRS patients.

In this study, we investigated the histopathological and radiographic changes associated with neo-osteogenesis and explored the relationship between interleukin (IL)-13 and runt-related transcription factor 2 (RUNX2) in a previously introduced murine eosinophilic NP model.

MATERIALS AND METHODS

Animals and tissue preparations

For all experiments, BALB/c male mice (4 weeks old, 24–25 g) were purchased (Central Laboratory Animals, Seoul, Korea) and kept for 1 week in specific pathogen-free rooms before initiating experiments. All experiments involving animals were approved by the

Institutional Animal Care and Use Committee of Seoul National University and complied with governmental and international guidelines on animal experimentation. We utilized the murine NP model following previous reports with some modifications.[22,23] For induction of NP in mouse nasal cavity, mice were sub-divided into the control group (n = 14) and the experimental group (n = 20), and treated with either phosphate-buffered saline (PBS) or 3% ovalbumin (OVA) plus 10 ng of staphylococcal enterotoxin B (SEB). For treatments with resveratrol (RSV) and dexamethasone, mice were categorized into a control group (group A; n = 6) and three experimental groups (groups B, C, and D; n = 12, 7, and 7, respectively). After treating with 3% OVA for 47 days, mice were administered RSV (0.44 μg per nostril) 3 times a week for 8 consecutive weeks. Dexamethasone (1 mg/kg) was delivered once a week for 8 consecutive weeks. The 3% OVA and SEB were applied before administrating the drugs. Mice were sacrificed 1 day after the last treatment. PBS was applied for both systemic and local stimulation in group A. Mouse sinonasal tissue specimens for various types of analysis were prepared as previously described.[24]

Micro-CT-based evaluation of bone thickness

The skull of each mouse (n = 3 from each group) was subjected to micro-CT (NFR-Polaris-G90; NanoFocusRay, Jeonju, Korea). Cross-sectional images were converted to the Digital Imaging and Communications in Medicine format using PMOD software (PMOD Technologies LLC, Zurich, Switzerland). For neo-osteogenesis evaluation, the same coronal plane showing the true maxillary sinuses and ethmoid labyrinths was selected for each mouse. The nasal bone thickness was measured at 5 different points on both right and left lateral walls and evaluated using Image J software (version 1.52p, National Institutes of Health [NIH] Image processing analysis, http://rsb.info.nih.gov/ij/).

Histopathological analysis and immunohistochemistry of animal tissues

Detailed experimental procedures for processing the sinonasal tissues and immunohistochemistry were previously described.[24,25] Briefly, the heads of mice were fixed in 4% PFA (Biosesang, Seongnam, Korea), decalcified in 5% nitric acid (Sigma-Aldrich, St. Louis, MO, USA), dehydrated, processed according to standard paraffin-embedding procedures, and coronally sectioned into 3-μm-thick sections. An atlas of normal murine sinonasal anatomy was used to standardize the anatomic locations being examined.[26] Several stains were conducted to compare characteristics between groups: hematoxylin and eosin (H&E; Sigma-Aldrich) for general morphology, Sirius red (Polysciences Inc., Warrington, PA, USA) for eosinophils, Giemsa (Sigma-Aldrich) stain for mast cells, periodic Acid-Schiff (Sigma-Aldrich) stain for goblet cells, and Masson's trichrome (Sigma-Aldrich) stain to highlight collagen deposition in the sub-epithelial layer, following the manufacturer's instructions. For immunohistochemistry, sections were stained with RUNX2, osteonectin, and IL-13 antibodies. Detailed information is indicated in **Supplementary Table S1**. The sections were then incubated with broad antibody enhancer and polymer-horseradish peroxidase (HRP) using polink-2 plus polymerized HRP broad 3,3′-Diaminobenzidine (DAB) Detection System (Golden Bridge International Labs., Bothell, WA, USA) following the manufacturer's recommendations. Five areas from nasal tissue sections were chosen randomly for evaluation under high-powered fields (HPFs; magnification ×1,000) and measured by 2 examiners who were blinded to group assignment. The numbers of NPs were counted following the previous standards,[24] quantified microscopically from 5 coronal sections, and presented as total number. The numbers of eosinophils, mast cells, and goblet cells were shown as the average numbers from 5 HPFs. Sub-epithelial fibrosis was evaluated as previously described.[27] For the assessment of bone thickness, at least 5 measurements at

different points were made in the appropriate area of each HPF (×400 magnification), and measured using Image J software (version 1.52p, NIH Image processing analysis, http://rsb.info.nih.gov/ij/).

Immunofluorescence (IF) staining and confocal microscopy

For IF staining, the tissue sections were processed as described previously.[24] Briefly, mouse nasal tissues were de-paraffinized, rehydrated, boiled in citrate buffer (Dako, Carpinteria, CA, USA) for epitope retrieval, fixed in 4% paraformaldehyde (PFA; Biosesang, Seongnam, Korea), washed 3 × 5 minutes in PBS containing 0.2% Triton X-100 (PBST), blocked in PBST containing 5% bovine serum albumin (BSA) (BSA-PBST) for 3 hours, incubated with primary antibodies diluted in BSA-PBST (Sigma-Aldrich) overnight at 4°C, washed 3 × 5 minutes with PBST, stained with secondary antibodies in BSA-PBST for 1 hour in the dark at room temperature, washed 3 × 5 minutes with PBST, stained with 4′,6-Diamidino-2-phenylindole (Sigma-Aldrich) for 15 minutes at room temperature, mounted with fluorescence-mounting medium (Vector Laboratories Inc., Burlingame, CA, USA). The primary antibodies utilized are summarized in **Supplementary Table S1**. Images were acquired with a Zeiss fluorescent microscope using AxioVision software (Carl Zeiss Vision, Thornwood, NY, USA). The images were edited using Zen Blue software (Zeiss, Oberkochen, Germany). Immunostaining was not observed in control sections incubated with normal serum instead of the primary antibodies (data not shown).

RNA extraction and quantitative real-time polymerase chain reaction (PCR)

Total RNA was collected from the tissue samples using QIAshredder and RNeasy Plus Mini kit (both Qiagen, Redwood City, CA, USA) following the manufacturer's recommendations. Total RNA (1 μg) was reverse transcribed to cDNA using the Tetro cDNA-synthesis kit (Bioline, Eveleigh, Australia) following the manufacturer's instructions. Quantitative real-time PCR was performed as previously described.[24] Briefly, polymerase chain reaction was conducted with SYBR Green Polymerase Chain Reaction Master Mix (Enzynomics, Daejeon, Korea) and primers that specifically amplify genes for *IL13*, *RUNX2*, matrix metallopeptidase 9 (*MMP9*), collagen type 1 (*COL1A1*), and osteopontin (*SPP1*). Additionally, β-actin (ACTB) was used as reference gene for normalization. The relative fold changes were calculated by the comparative $2^{-\Delta\Delta Cq}$ method. The primer sequences used in this study are described in **Supplementary Table S2**. Cycling conditions were 95°C for 10 minutes, followed by 40 cycles at 95°C for 10 seconds, 60°C for 1 minutes, and 72°C for 30 seconds. The PCR efficiency in all runs was close to 100%, and all samples were tested in duplicate.

Bioinformatic analysis

The normalized dataset (GSE23552), which contains 13 normal nasal mucosal tissues and 26 CRS microarray data, was imported from Gene Expression Omnibus (www.ncbi.nih.gov/geo). All tissues (n = 39) were divided into 3 groups: normal tissues (n = 13), chronic rhinosinusitis without nasal polyp (CRSsNP) tissues (n = 15), chronic rhinosinusitis with nasal polyp (CRSwNP) tissues (n = 11). The values of 2828688 (corresponding to *IL13*), 2908762 (corresponding to *RUNX2*), 3887210 (corresponding to *MMP9*), 3762198 (corresponding to *COL1A1*), and 2735027 (corresponding to *SPP1*) on each group were calculated and compared between the 3 groups using Spearman's correlation analysis. Enrichment analysis was also performed using Gene Set Enrichment Analysis (GSEA) software v3.0 and a formatted GCT file was used as input for the GSEA algorithm (available from: http://www.broadinstitute.org/gsea). For grouping the GSE23552 dataset, the value of the 2828688 probe was utilized as criteria for high expression group and low expression

groups. In the analysis, pre-defined osteogenesis-related gene sets in the Gene Ontology collection (GO) from v6.2 molecular signature database (mSigDB c5 category; http://software.broadinstitute.org/gsea/msigdb) were used, and the number of permutations was set at 1,000. The gene sets with $P < 0.05$ and false discovery rate (FDR) < 0.25 were considered significantly enriched.

Statistical analysis

Data are expressed as mean ± standard errors (SEs) from 2 or more distinct samples unless indicated otherwise. We used unpaired Student's *t*-test (2-sided) or non-parametric Mann-Whitney *U* test (2-tailed) to compare differences between groups. In addition, correlations of protein or mRNA expression were determined using Spearman's *P* statistic or Pearson's *P* statistic. Statistical analyses were performed using SPSS 23.0 software (SPSS, Chicago, IL, USA). Illustrative figures were generated using Prism version 8.2.0 (GraphPad Software Inc., San Diego, CA, USA) and SigmaPlot version 10.0 (Systat Software Inc., San Jose, CA, USA).

RESULTS

Histopathological evidence of neo-osteogenesis in the eosinophilic CRSwNP model

To evaluate neo-osteogenesis in mice, we employed an experimental CRSwNP murine model based on previous reports with some modifications (**Fig. 1A**).[24,25,28] Because NPs are associated with osteitis severity and bone remodeling,[29] we first checked the number of NPs in mouce nasal cavity. As expected, thickened mucosae with polyp-like lesions were found in the OVA/SEB-treated group, whereas no signs of inflammation were observed in control mice (**Supplementary Fig. S1A**). When we assessed sub-epithelial fibrosis, eosinophils numbers, mast cells numbers, and goblet cells numbers, following the previous report,[30] we observed similar results (**Supplementary Fig. S1B-E**). In order to find evidence of bone remodeling, we next examined the number of osteoblasts and osteoclasts which are responsible for bone formation and bone resorption, respectively. We detected not only an increased number of osteoblasts and osteoclasts at the rim of the bone but also a woven bone with marked thickening periosteum in OVA/SEB-treated mice (**Fig. 1B-D**). The micro-CT findings exhibited areas of up-regulated bone thickness and irregular thickening of the sinus walls in OVA/SEB-treated mice. (**Fig. 1E and F**).

Increased RUNX2 expression in eosinophilic CRS with neo-osteogenesis

New bone formation is mainly mediated by mature osteoblasts. In this process, RUNX2 serves as master regulator and induces the differentiation of pre-osteoblast.[31] Therefore, we inspected the expression of RUNX2 and the number of mature osteoblasts by using immunohistochemistry. We found that RUNX2-immunoreactive cells were significantly elevated in OVA/SEB-treated mice. RUNX2-immunoreactivity was particularly identified in osteoblasts lining the bone (**Fig. 2A and B**). The mature osteoblasts on the bone surface were evaluated on the basis of the expression of osteonectin (a differentiation marker for bone cells), as shown in **Fig. 2A and C**. By utilizing IF staining, we observed marked co-localization of RUNX2 and osteonectin mainly lining the bone in mice nasal tissues, as previously reported (**Fig. 2C**). Because RUNX2-induced differentiated osteoblasts induce osteogenesis, we compared the relationship between RUNX2 level and bone thickness. A significant positive correlation was detected between bone thickness and RUNX2-positive cell numbers (**Fig. 2D**; Pearson's correlation coefficient, $P < 0.01$). These results suggest that OVA/SEB-treated mice showed neo-osteogenic characteristics.

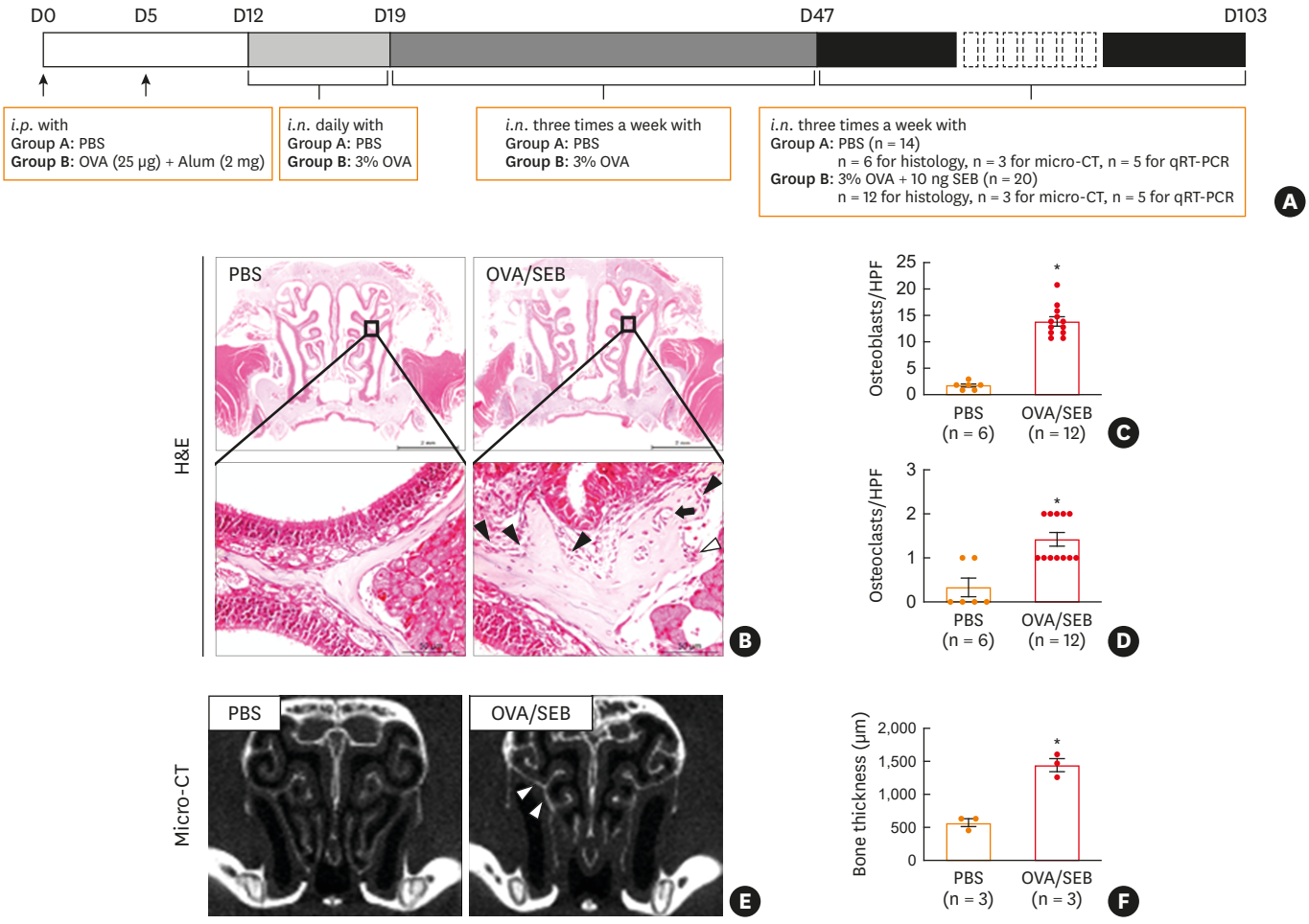

Fig. 1. Establishment of eosinophilic CRS with neo-osteogenesis murine model. (A) A schematic representation of the study protocol. (B) Representative images of decalcified tissue specimens showing histological evidence of neo-osteogenesis in mice. Insets in (B) show a magnified view of the outlined area (bottom). The rows of osteoblasts (arrowhead) at the rim of bone were noted. The white arrowhead indicates an osteoclast, while the black arrow indicates a Haversian canal. Original magnification ×2.5 (above) and insets ×40 (bottom). (C, D) The numbers of osteoblasts and osteoclasts per HPF were quantified in indicated groups. (E) Micro-CT evaluation of bony changes. Evidence of bone thickening (arrowhead) was found in the OVA/SEB-treated group. (F) Histo-morphometric analyses showed upregulation of bone thickness in the OVA/SEB-delivered group. All results are presented as mean ± SEM. Individual values are indicated by dots (C, D, F). Statistical significance was determined by Mann-Whitney *U* test for pairwise comparisons (C, D, F).
OVA, ovalbumin; SEB, staphylococcal enterotoxin B; PBS, phosphate-buffered saline; *i.p.*, intraperitoneal; *i.n.*, intranasal; HPF, high-powered field; CT, computed tomography; SEM, standard error of the mean.
*$P < 0.01$.

Increased IL-13 expression in eosinophilic CRS with neo-osteogenesis

We previously found that IL-13, one of the representative Th2 cytokines, induced neo-osteogenesis via RUNX2 expression.[32] To verify this in our murine model, we evaluated the expression of IL-13. Immunohistochemistry studies revealed that IL-13 expression, in mucosal tissues overlying the bone, was increased in the OVA/SEB-treated mice compared to the PBS-treated mice (**Fig. 3A and B**). The number of IL-13-positive cells positively correlated with the number of RUNX2-positive cells (**Fig. 3C**; Pearson's correlation coefficient, $P < 0.01$). Moreover, IL-13-positive cell numbers showed positive association with bone thickness (**Fig. 3D**; Pearson's correlation coefficient, $P < 0.05$). Furthermore, mRNA expression levels of IL-13, RUNX2, and RUNX2 downstream genes (*MMP9*, *COL1A1*, and *SPP1*) were also increased in OVA/SEB-treated mice (**Fig. 3E**). This result indicates that IL-13, which was secreted during stimulation with OVA/SEB, could contribute to ossification via RUNX2, suggesting the possibility of osteogenesis in mice.

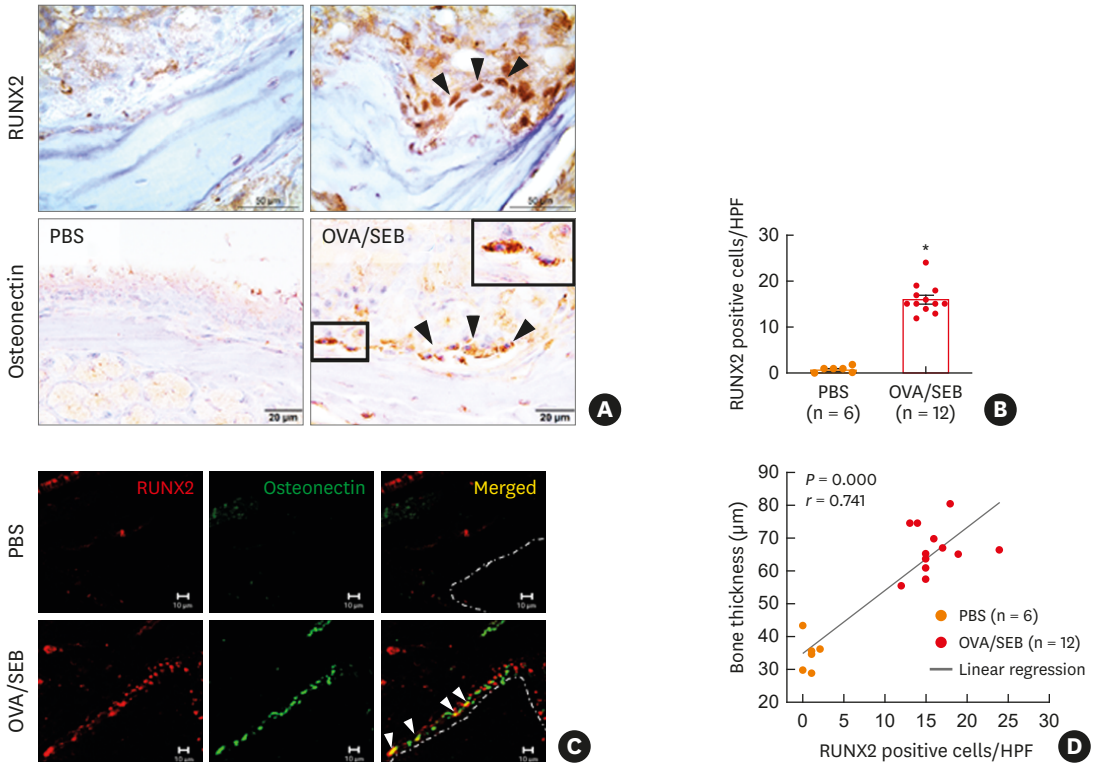

Fig. 2. OVA and SEB induced the expression of RUNX2 and osteonectin. (A) Representative photographs of immune-histochemical staining against RUNX2 (above) and osteonectin (bottom). Insets in (A) present a magnified view of the outlined area, and arrowheads denote representative positive cells (scale bar = 50 μm in above and scale bar = 20 μm in bottom). (B) The numbers of RUNX2-positive cells per HPF were counted in each group. (C) Co-localization of RUNX2 (red) and osteonectin (green) in nasal tissues revealed by immunofluorescence staining. Arrowheads indicate RUNX2 and osteonectin-double positive cells (yellow) (scale bar = 10 μm). (D) Relationship between bone thickness and RUNX2-positive cells. All results are presented as mean ± SEM. Individual values are indicated by dots (B, D). Statistical significance was determined by Mann-Whitney *U* test for pairwise comparisons (B). Pearson's *r* values and the corresponding *P*-values were determined by Pearson's correlation test (D).
OVA, ovalbumin; SEB, staphylococcal enterotoxin B; RUNX2, runt-related transcription factor 2; HPF, high-powered field; SEM, standard error of the mean.
$^{*}P < 0.01$.

Positive correlations between IL-13 and RUNX2 downstream genes in human CRS transcriptome

To verify the role of IL-13 in human nasal tissues, we conducted bioinformatic analysis using a previously published dataset (GSE23552). CRS patient tissues in the GSE23552 data set were categorized into *IL13*_high and *IL13*_low groups based on the median *IL13* expression value to find gene expression signatures that correlated with *IL13* expression (**Fig. 4A**). Importantly, many osteogenesis-related gene sets were enriched in the *IL13*_high group (**Fig. 4B**; $P < 0.05$, FDR < 0.25). **Fig. 4C** showed 2 representative enrichment plots of gene sets. Enrichment plots that were identified in **Fig. 4B** were indicated in **Supplementary Fig. S2**. We then compared the mRNA levels of *IL13*, *RUNX2*, and *RUNX2* downstream genes between normal nasal tissues and CRS patient tissues. *IL13* expression levels were higher in CRSwNP tissues than in normal nasal tissues. Similarly, transcript expression levels of RUNX2 and RUNX2 downstream target genes (*SPP1*, *MMP9*, and *COL1A1*) were also up-regulated in both CRSsNP and CRSwNP tissues (**Fig. 4D**). Spearman correlation analysis showed that *IL13* expression positively correlated with *SPP1* and *MMP9* expression (**Fig. 4E**; Spearman's correlation coefficient, $P < 0.05$ and $P < 0.01$, respectively).

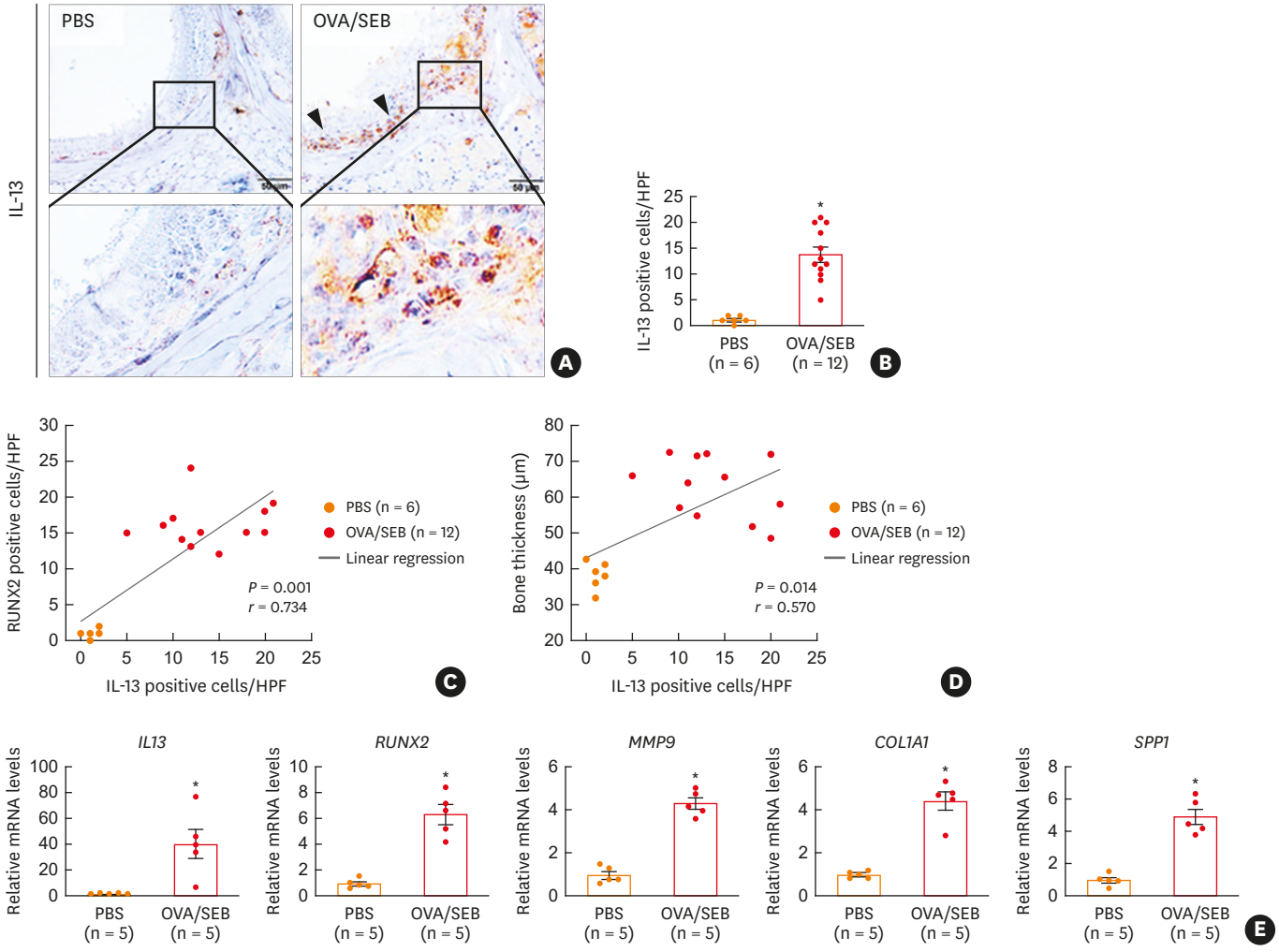

Fig. 3. OVA and SEB upregulated the expression of IL-13 and showed positive correlations with RUNX2 downstream genes. (A) Representative images of immunehistochemical staining against IL-13 (original magnification ×400). Insets in (A) show a magnified view of the outlined area, and arrowheads denote IL-13-positive cells (scale bar = 50 μm). (B) The number of IL-13-positive cells per HPF was counted and compared to the control group. Correlation of the number of IL-13-positive cells and the number of RUNX2-positive cells (C) or the number of IL-13-positive cells and bone thickness (D) in each group of mice. (E) Relative mRNA expressions of *IL13*, *RUNX2*, and *RUNX2* downstream genes (*MMP9*, *COL1A1*, and *SPP1*) in mucosal tissues from mice were compared. All results are presented as means ± SEM. Individual values are indicated by dots (B-E). Statistical significance was determined by Mann-Whitney *U* test for pairwise comparisons (B, E). Pearson's *r* values and the corresponding *P*-values were determined by Pearson's correlation test (C, D).
OVA, ovalbumin; SEB, staphylococcal enterotoxin B; IL, interleukin; RUNX2, runt-related transcription factor 2; HPF, high-powered field; *MMP9*, matrix metallopeptidase 9; *COL1A1*, collagen type 1; *SPP1*, osteopontin; SEM, standard error of the mean; PBS, phosphate-buffered saline.
*$P < 0.01$.

RSV treatment diminished osteogenesis in eosinophilic CRS NP model

Finally, we deployed this eosinophilic murine NP model to evaluate the therapeutic effect of a drug candidate against osteitis (**Fig. 5A**). For this purpose, we used RSV and dexamethasone which are previously known to reduce NPs.[28,30] When we applied these drugs to the OVA/SEB-treated mice, we found decreased numbers of osteoblasts and bone thickness comparable to the PBS-treated mice (**Fig. 5B**). The expression of RUNX2-positive cells was diminished by the treatment of RSV and dexamethasone (**Fig. 5C**). A similar finding was observed regarding IL-13 (**Supplementary Fig. S3**). This result implies that our eosinophilic murine NP model might be applicable to evaluating the effects of some type of drugs targeting osteitis in terms of CRS.

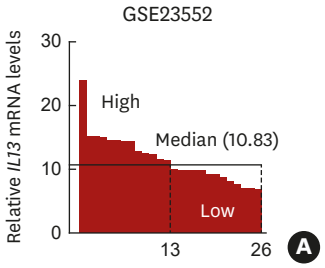

NAME [gene sets related to osteogenesis]	ES	NES	Nom *P*-value	FDR q-value
GO_REGULATION_OF_BONE_REMODELING	0.59	2.02	0.00	0.00
GO_REGULATION_OF_BONE_RESORPTION	0.65	1.97	0.00	0.00
GO_BONE_REMODELING	0.60	1.75	0.00	0.03
GO_REGULATION_OF_BONE_DEVELOPMENT	0.53	1.59	0.02	0.09
GO_BONE_RESORPTION	0.62	1.58	0.03	0.08
GO_OSTEOCLAST_DIFFERENTIATION	0.57	1.55	0.02	0.08
GO_REGULATION_OF_OSTEOCLAST_DIFFERENTIATION	0.45	1.53	0.04	0.08
GO_NEGATIVE_REGULATION_OF_OSTEOCLAST_DIFFERENTIATION	0.48	1.49	0.05	0.10

B

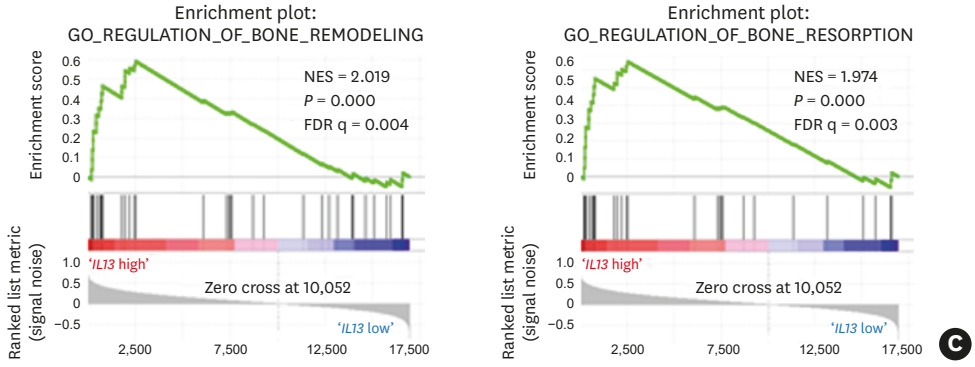

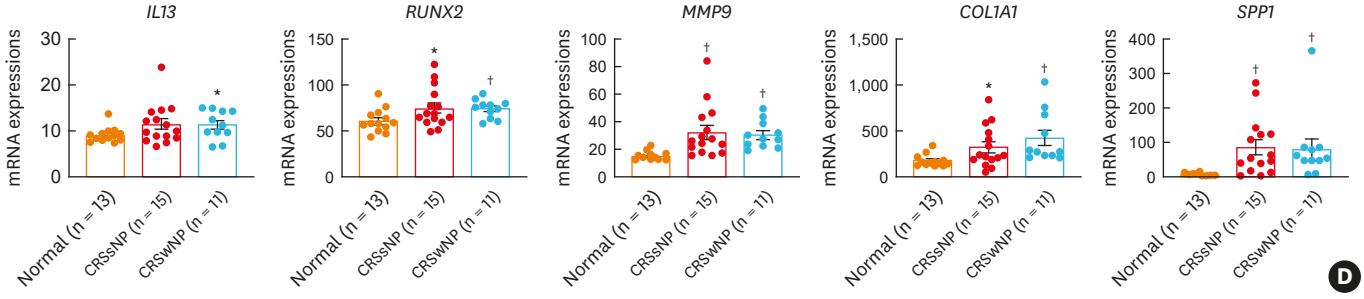

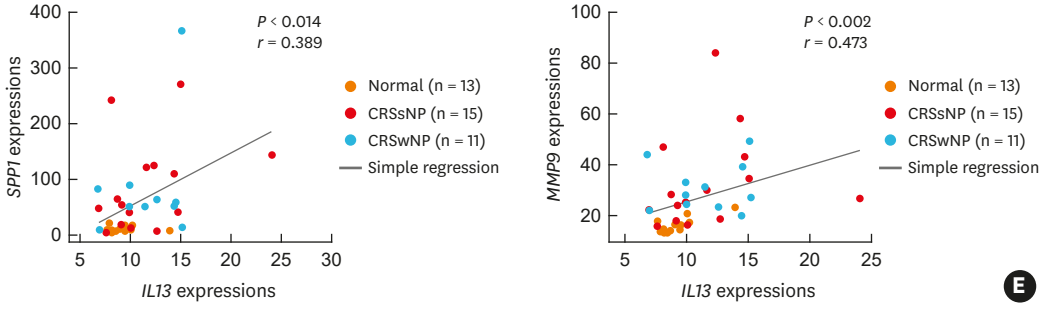

Fig. 4. IL-13 is upregulated in CRS patients and positively correlated with osteogenesis-related genes. (A) Distribution of *IL13* mRNA levels in 26 human CRS nasal tissues (data set GSE23552). Based on the median value, the CRS patients with or without NPs were categorized into high and low groups. The number of CRS tissues are *IL13* high group (n = 13) and *IL13* low group (n = 13). (B) GSEA. osteogenesis-related gene sets were selected in the GO collection from MSigDB v6.2. The 8 gene sets which show a positive correlation with *IL13* are presented ($P < 0.05$ and FDR < 0.25). (C) Representative enrichment plots of the GSEA analysis in the GSE23552 data set. (D) Relative mRNA levels of IL-13, RUNX2 and RUNX2 downstream genes in the nasal tissues obtained from the GSE23552 data set. (E) Correlation between *IL13* and *SPP1* or *IL13* and *MMP9*. Spearman's correlation analysis was performed in each group of subjects. All results are presented as means ± SEM. Individual values are indicated by dots (D, E). Statistical significance was determined by Kruskal-Wallis tests ($P < 0.01$), followed by Mann-Whitney *U* test for pairwise comparisons (D). Spearman's *r* values and the corresponding *P*-values were determined by spearman's correlation test (E).
IL, interleukin; CRS, chronic rhinosinusitis; NP, nasal polyp; GSEA, Gene Set Enrichment Analysis; GO, Gene Ontology; FDR, false discovery rate; RUNX2, runt-related transcription factor 2; *SPP1*, osteopontin; *MMP9*, matrix metallopeptidase 9; SEM, standard error of the mean; ES, enrichment score; NES, normalized enrichment score; *COL1A1*, collagen type 1; CRSsNP, chronic rhinosinusitis without nasal polyp; CRSwNP, chronic rhinosinusitis with nasal polyp.
$^{*}P < 0.05$; $^{\dagger}P < 0.01$.

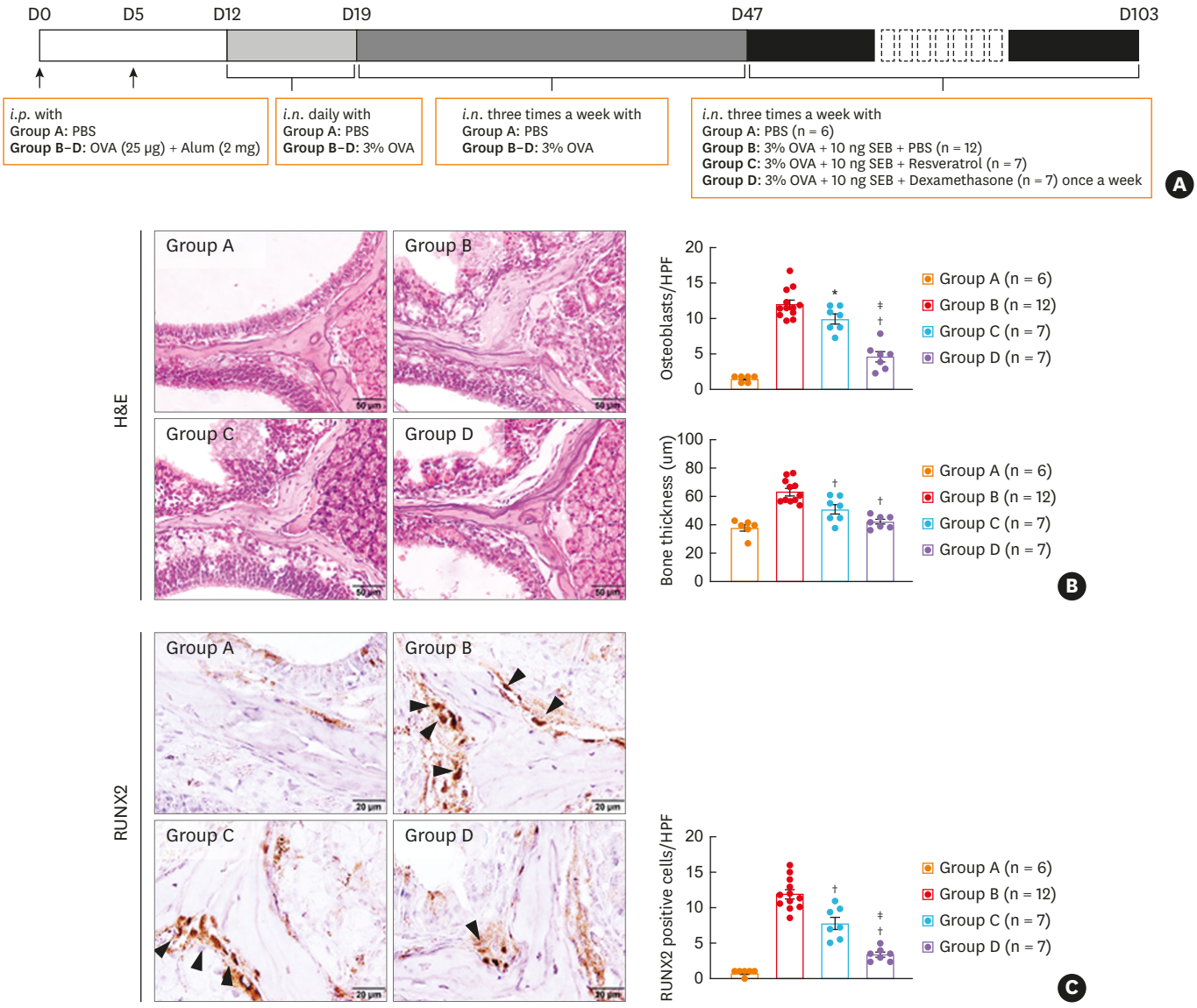

Fig. 5. Resveratrol suppresses the new bone formation in neo-osteogenesis murine model. (A) A schematic illustration of the study procedure. (B) Representative H&E photographs of nasal tissue specimens (left). The number of osteoblasts and bone thickness per HPF were quantified in specified groups and compared (scale bar = 50 μm). (C) Cells showing RUNX2 positivity per HPF were counted in designated groups and compared (scale bar = 20 μm). All results are presented as means ± SEM. Individual values are indicated by dots (B, C). Statistical significance was determined by Kruskal-Wallis tests ($P < 0.01$), followed by Mann-Whitney *U* test for pairwise comparisons (B, C).
H&E, hematoxylin and eosin; HPF, high-powered field; RUNX2, runt-related transcription factor 2; OVA, ovalbumin; SEB, staphylococcal enterotoxin B; PBS, phosphate-buffered saline; *i.p.*, intraperitoneal; *i.n.*, intranasal.
Significant differences are denoted relative to group B (OVA/SEB-applied group) ($^{*}P < 0.05$; $^{\dagger}P < 0.01$) or to group C (Resveratrol-treated group) ($^{\ddagger}P < 0.01$).

DISCUSSION

Current experimental animal models allow to investigate the role of osteitis in the context of CRS pathogenesis, but none of these models are effective in exploring the in-depth mechanisms of osteitis, suggesting the necessity of a more suitable pathogenic model. In this study, we provide evidence of new bone formation or neo-osteogenesis in a previously established eosinophilic CRSwNP murine model.[22] OVA/SEB-administration in mice showed histopathological changes

in the sinonasal tissues including the infiltration of immune cells, fibrosis, periosteal thickening, increased osteoblastic activity and woven bone formation (**Fig. 1** and **Supplementary Fig. S1**). We found not only elevated levels of RUNX2 and IL-13, but also positive correlation between RUNX2 positive cells and IL-13 positive cells. Bone thickness positively correlated with the numbers of IL-13 and RUNX2 positive cells (**Figs. 2D** and **3D**). In addition, the expression of IL-13 presented significant positive correlation with osteogenesis-related gene sets in the human CRS transcriptome (**Fig. 4** and **Supplementary Fig. S2**). We finally evaluated the effects of RSV in this murine model and observed a reduction in osteogenesis, evidenced by the expression of IL-13, RUNX2 and histopathological findings following RSV treatment (**Fig. 5**). Thus, this model can be utilized as a potential murine model for investigating the role of certain proteins or evaluating the effect of drugs in terms of osteogenesis.

The balance of osteoclasts and osteoblasts, responsible for bone homeostasis, is tightly controlled and requires multiple cellular participants. In the process of bone remodeling, bone resorption is initiated by osteoclasts, and then osteoblasts coordinate bone formation by synthesizing multiple bone matrix related proteins.[33] RUNX2 (core-binding factor subunit alpha-1) plays an essential role in the proliferation and differentiation of osteoblasts, and regulates the expression of several osteoblastic genes including *COL1A1*, osteocalcin (*BGLAP*), *SPP1*, and *MMP9*.[34] However, various studies have reported that an inflammatory milieu disrupted the balance between osteoblasts and osteoclasts, and led to pathogenic conditions such as abnormal bone loss or bone development.[35,36] In the context of severe sinonasal mucosal inflammation, the balance between bone formation and bone resorption might be destroyed, resulting in osteogenesis or bone remodeling. Actually, our study showed an increased number of osteoblasts and osteoclasts as well as elevated numbers of RUNX2-positive cells in OVA/SEB-treated mice (**Fig. 1B-D** and **Fig. 2A-C**). We also showed that RUNX2 downstream genes, such as *MMP9*, *COL1A1*, and *SPP1*, are up-regulated following OVA/SEB treatment, which suggests osteogenesis (**Fig. 3E**).

Eosinophils produce Th2 cytokines (IL-4, IL-5, and IL-13) and are implicated in the pathogenesis of allergic inflammatory diseases including eosinophilic CRSwNP or CRSsNP.[3,37] The association between eosinophilia and osteitis severity in CRS has been demonstrated.[9,16,38] Among the eosinophil-activating cytokines, the role of IL-13 in neo-osteogenesis has been suggested in several studies, and it has been hypothesized that IL-13 regulates the activity of osteoblasts and osteoclasts.[39-41] In a recent study, we found that IL-13 contributes to new bone formation and could affect bone remodeling in CRS patients by inducing RUNX2.[32] Shi *et al.* showed that IL-13 promotes the expression of RUNX2 in human bronchial epithelial cells.[42] These findings imply that IL-13 plays a role in osteoblast differentiation by enhancing the expression of RUNX2, which is a key transcription factor in the early stage of osteogenic differentiation. As previously reported, eosinophilic murine NP model showed the polyp-like lesions along with increased levels of Th2 cytokines including IL-4, IL-5, and IL-13.[22] Therefore, we speculated that OVA/SEB-treated mice may present features of neo-osteogenesis. Here, we observed not only up-regulation of IL-13 and RUNX2, but also the positive association between IL-13 expression and RUNX2 levels, proposing signs of osteogenesis in the eosinophilic murine NP model.

Treatment with OVA alone was insufficient to induce epithelial remodeling in the sinonasal tissue of mice (data not shown). However, administration of 3% OVA with a low dose of SEB (10 ng per nostril) was enough to induce nasal polypoid lesions with epithelial remodeling, showing increased infiltration of immune cells and higher levels of Th2 inflammatory

cytokines.[22] Bone remodeling or erosion is observed in sinonasal polyposis with high levels of Th2 inflammatory cytokines, implying osteogenesis in our murine NP model.

RSV is highly abundant in peels of red grapes and blueberries, and largely used for protective effects against inflammation.[43] Recent reports have suggested the anti-inflammatory effect of resveratrol.[44,45] We previously observed that resveratrol (previously known as SIRT1 activator) administration in mouse nasal cavity significantly reduced nasal polyp numbers as well as protein expression of inflammatory cytokines and infiltrated immune cells.[28] Another study also showed the beneficial effect of resveratrol in decreasing nasal polyps in mice.[46] Considering that an inflammatory milieu is favorable to bone formation, we speculate that resveratrol treatment may alleviate osteogenesis. In this study, we investigated the role of resveratrol in the context of osteitis, and found the reduction of bone formation or remodeling of bone in mice, suggesting the applicability of this murine model for investigating the efficiency of drugs targeting CRS patients with osteogenesis.

The murine model was chosen because it has been the most commonly studied animal model for chronic rhinosinusitis.[27,46-48] Furthermore, it has several advantages over the rabbit pathogenic model; including lower housing cost, simple genetic manipulation and availability of various murine reagents. However, there are 2 limitations in this study that could be addressed in future research. First, bone mineralization is a highly ordered process by which the organic bone matrix becomes saturated with calcium phosphate nanocrystals and is considered an important factor to assess bone remodeling.[49] Although we detected the up-regulation of osteoblasts and bone thickness in OVA/SEB-treated mice (**Fig. 1C and D**, **Fig. 5B**), we could not quantify the degree of bone mineralization in our study due to embedding procedures which involved the removal of calcium deposits. Secondly, OVA from egg is a basic food component, not an airborne allergen. Although our eosinophilic NP murine model can mimic human CRS conditions, future studies using real allergens, such as house dust mite, have to be conducted.

In conclusion, we report histopathological and radiographic evidence of new bone formation or neo-osteogenesis in a murine model of eosinophilic CRSwNP. Resveratrol delivery sufficiently reduced osteogenesis in mice. This animal model could bring new insights into the pathophysiology of neo-osteogenesis and provides a basis for developing new therapeutics targeting osteitis.

ACKNOWLEDGMENTS

This work was supported by a grant of the Korea Health Technology R&D Project through the Korea Health Industry Development Institute (KHIDI), funded by the Ministry of Health & Welfare, Republic of Korea (grant number: HI17C1669, to H.W.S.).

SUPPLEMENTARY MATERIALS

Supplementary Table S1

List of antibodies used in this study

Click here to view

Supplementary Table S2

The quantitative polymerase chain reaction primers used in this study

Click here to view

Supplementary Fig. S1

Histopathological evaluation of nasal mucosal tissue. (A) Representative H&E-stained photographs of sinonasal spaces and polyp like lesions. (B) Sub-epithelial fibrosis. (C) The number of eosinophils. (D) The number of mast cells. (E) The number of goblet cells. All results are presented as means ± SEM. Individual values are indicated by dots (A-E). Statistical significance was determined by Mann-Whitney *U* test for pairwise comparisons (A-E). Scale bars are 20 μm (A) and 50 μm (B-D).

Click here to view

Supplementary Fig. S2

IL-13 is positively associated with high expression of osteogenesis-related gene sets. Enrichment plots of the top 8 gene sets that were positively correlated with IL-13 expression ($P < 0.05$ and FDR < 0.25).

Click here to view

Supplementary Fig. S3

The number of IL-13 positive cells and correlation with RUNX2 positive cells. (A) The cells showing IL-13 positivity are counted per HPF were counted in indicated groups and compared (scale bar = 20 μm). (B) Relationship between IL-13 positive cells and RUNX2-positive cells. Results are presented as means ± SEM. Individual values are indicated by dots (A). Statistical significance was determined by Kruskal-Wallis tests ($P < 0.01$), followed by Mann-Whitney *U* test for pairwise comparisons (A). Spearman's *r* values and the corresponding *P*-values were determined by spearman's correlation test (B).

Click here to view

REFERENCES

1. Hamilos DL. Chronic rhinosinusitis: epidemiology and medical management. J Allergy Clin Immunol 2011;128:693-707.
   PUBMED | CROSSREF
2. Stevens WW, Lee RJ, Schleimer RP, Cohen NA. Chronic rhinosinusitis pathogenesis. J Allergy Clin Immunol 2015;136:1442-53.
   PUBMED | CROSSREF
3. Fokkens WJ, Lund VJ, Mullol J, Bachert C, Alobid I, Baroody F, et al. EPOS 2012: European position paper on rhinosinusitis and nasal polyps 2012. A summary for otorhinolaryngologists. Rhinology 2012;50:1-12.
   PUBMED | CROSSREF
4. Kim YS, Han D, Kim J, Kim DW, Kim YM, Mo JH, et al. In-depth, proteomic analysis of nasal secretions from patients with chronic rhinosinusitis and nasal polyps. Allergy Asthma Immunol Res 2019;11:691-708.
   PUBMED | CROSSREF
5. Bhandarkar ND, Sautter NB, Kennedy DW, Smith TL. Osteitis in chronic rhinosinusitis: a review of the literature. Int Forum Allergy Rhinol 2013;3:355-63.
   PUBMED | CROSSREF

6. Kennedy DW, Senior BA, Gannon FH, Montone KT, Hwang P, Lanza DC. Histology and histomorphometry of ethmoid bone in chronic rhinosinusitis. Laryngoscope 1998;108:502-7.
PUBMED | CROSSREF
7. Perloff JR, Gannon FH, Bolger WE, Montone KT, Orlandi R, Kennedy DW. Bone involvement in sinusitis: an apparent pathway for the spread of disease. Laryngoscope 2000;110:2095-9.
PUBMED | CROSSREF
8. Giacchi RJ, Lebowitz RA, Yee HT, Light JP, Jacobs JB. Histopathologic evaluation of the ethmoid bone in chronic sinusitis. Am J Rhinol 2001;15:193-7.
PUBMED | CROSSREF
9. Snidvongs K, McLachlan R, Chin D, Pratt E, Sacks R, Earls P, et al. Osteitic bone: a surrogate marker of eosinophilia in chronic rhinosinusitis. Rhinology 2012;50:299-305.
PUBMED | CROSSREF
10. Lee JT, Kennedy DW, Palmer JN, Feldman M, Chiu AG. The incidence of concurrent osteitis in patients with chronic rhinosinusitis: a clinicopathological study. Am J Rhinol 2006;20:278-82.
PUBMED | CROSSREF
11. Videler WJ, Georgalas C, Menger DJ, Freling NJ, van Drunen CM, Fokkens WJ. Osteitic bone in recalcitrant chronic rhinosinusitis. Rhinology 2011;49:139-47.
PUBMED | CROSSREF
12. Kim HY, Dhong HJ, Lee HJ, Chung YJ, Yim YJ, Oh JW, et al. Hyperostosis may affect prognosis after primary endoscopic sinus surgery for chronic rhinosinusitis. Otolaryngol Head Neck Surg 2006;135:94-9.
PUBMED | CROSSREF
13. Richtsmeier WJ. Top 10 reasons for endoscopic maxillary sinus surgery failure. Laryngoscope 2001;111:1952-6.
PUBMED | CROSSREF
14. Bhandarkar ND, Mace JC, Smith TL. The impact of osteitis on disease severity measures and quality of life outcomes in chronic rhinosinusitis. Int Forum Allergy Rhinol 2011;1:372-8.
PUBMED | CROSSREF
15. Georgalas C, Videler W, Freling N, Fokkens W. Global Osteitis Scoring Scale and chronic rhinosinusitis: a marker of revision surgery. Clin Otolaryngol 2010;35:455-61.
PUBMED | CROSSREF
16. Mehta V, Campeau NG, Kita H, Hagan JB. Blood and sputum eosinophil levels in asthma and their relationship to sinus computed tomographic findings. Mayo Clin Proc 2008;83:671-8.
PUBMED | CROSSREF
17. Khalid AN, Hunt J, Perloff JR, Kennedy DW. The role of bone in chronic rhinosinusitis. Laryngoscope 2002;112:1951-7.
PUBMED | CROSSREF
18. Bolger WE, Leonard D, Dick EJ Jr, Stierna P. Gram negative sinusitis: a bacteriologic and histologic study in rabbits. Am J Rhinol 1997;11:15-25.
PUBMED | CROSSREF
19. Norlander T, Forsgren K, Kumlien J, Stierna P, Carlsöö B. Cellular regeneration and recovery of the maxillary sinus mucosa. An experimental study in rabbits. Acta Otolaryngol Suppl 1992;492:33-7.
PUBMED | CROSSREF
20. Westrin KM, Norlander T, Stierna P, Carlsöö B, Nord CE. Experimental maxillary sinusitis induced by Bacteroides fragilis. A bacteriological and histological study in rabbits. Acta Otolaryngol 1992;112:107-14.
PUBMED | CROSSREF
21. Antunes MB, Feldman MD, Cohen NA, Chiu AG. Dose-dependent effects of topical tobramycin in an animal model of Pseudomonas sinusitis. Am J Rhinol 2007;21:423-7.
PUBMED | CROSSREF
22. Kim DW, Khalmuratova R, Hur DG, Jeon SY, Kim SW, Shin HW, et al. Staphylococcus aureus enterotoxin B contributes to induction of nasal polypoid lesions in an allergic rhinosinusitis murine model. Am J Rhinol Allergy 2011;25:e255-61.
PUBMED | CROSSREF
23. Shin HW. Animal models in CRS and pathophysiologic insights gained: a systematic review. Laryngoscope Investig Otolaryngol 2016;1:116-23.
PUBMED | CROSSREF
24. Lee M, Kim DW, Khalmuratova R, Shin SH, Kim YM, Han DH, et al. The IFN-γ-p38, ERK kinase axis exacerbates neutrophilic chronic rhinosinusitis by inducing the epithelial-to-mesenchymal transition. Mucosal Immunol 2019;12:601-11.
PUBMED | CROSSREF

25. Lee M, Kim DW, Yoon H, So D, Khalmuratova R, Rhee CS, et al. Sirtuin 1 attenuates nasal polypogenesis by suppressing epithelial-to-mesenchymal transition. J Allergy Clin Immunol 2016;137:87-98.e7.
PUBMED | CROSSREF

26. Jacob A, Chole RA. Survey anatomy of the paranasal sinuses in the normal mouse. Laryngoscope 2006;116:558-63.
PUBMED | CROSSREF

27. Khalmuratova R, Lee M, Kim DW, Park JW, Shin HW. Induction of nasal polyps using house dust mite and Staphylococcal enterotoxin B in C57BL/6 mice. Allergol Immunopathol (Madr) 2016;44:66-75.
PUBMED | CROSSREF

28. Lee M, Park CG, Huh BK, Kim SN, Lee SH, Khalmuratova R, et al. Sinonasal delivery of resveratrol via mucoadhesive nanostructured microparticles in a nasal polyp mouse model. Sci Rep 2017;7:40249.
PUBMED | CROSSREF

29. Telmesani LM, Al-Shawarby M. Osteitis in chronic rhinosinusitis with nasal polyps: a comparative study between primary and recurrent cases. Eur Arch Otorhinolaryngol 2010;267:721-4.
PUBMED | CROSSREF

30. Khalmuratova R, Lee M, Mo JH, Jung Y, Park JW, Shin HW. Wogonin attenuates nasal polyp formation by inducing eosinophil apoptosis through HIF-1α and survivin suppression. Sci Rep 2018;8:6201.
PUBMED | CROSSREF

31. Raggatt LJ, Partridge NC. Cellular and molecular mechanisms of bone remodeling. J Biol Chem 2010;285:25103-8.
PUBMED | CROSSREF

32. Khalmuratova R, Shin HW, Kim DW, Park JW. Interleukin (IL)-13 and IL-17A contribute to neo-osteogenesis in chronic rhinosinusitis by inducing RUNX2. EBioMedicine 2019;46:330-41.
PUBMED | CROSSREF

33. Tanaka Y, Nakayamada S, Okada Y. Osteoblasts and osteoclasts in bone remodeling and inflammation. Curr Drug Targets Inflamm Allergy 2005;4:325-8.
PUBMED | CROSSREF

34. Komori T. Roles of Runx2 in skeletal development. Adv Exp Med Biol 2017;962:83-93.
PUBMED | CROSSREF

35. Loi F, Córdova LA, Pajarinen J, Lin TH, Yao Z, Goodman SB. Inflammation, fracture and bone repair. Bone 2016;86:119-30.
PUBMED | CROSSREF

36. Glowacki AJ, Yoshizawa S, Jhunjhunwala S, Vieira AE, Garlet GP, Sfeir C, et al. Prevention of inflammation-mediated bone loss in murine and canine periodontal disease via recruitment of regulatory lymphocytes. Proc Natl Acad Sci U S A 2013;110:18525-30.
PUBMED | CROSSREF

37. Khalmuratova R, Park JW, Shin HW. Immune cell responses and mucosal barrier disruptions in chronic rhinosinusitis. Immune Netw 2017;17:60-7.
PUBMED | CROSSREF

38. Wang M, Ye T, Liang N, Huang Z, Cui S, Li Y, et al. Differing roles for TGF-β/Smad signaling in osteitis in chronic rhinosinusitis with and without nasal polyps. Am J Rhinol Allergy 2015;29:e152-9.
PUBMED | CROSSREF

39. Silfverswärd CJ, Larsson S, Ohlsson C, Frost A, Nilsson O. Reduced cortical bone mass in mice with inactivation of interleukin-4 and interleukin-13. J Orthop Res 2007;25:725-31.
PUBMED | CROSSREF

40. Wang Y, Wu NN, Mou YQ, Chen L, Deng ZL. Inhibitory effects of recombinant IL-4 and recombinant IL-13 on UHMWPE-induced bone destruction in the murine air pouch model. J Surg Res 2013;180:e73-81.
PUBMED | CROSSREF

41. Onoe Y, Miyaura C, Kaminakayashiki T, Nagai Y, Noguchi K, Chen QR, et al. IL-13 and IL-4 inhibit bone resorption by suppressing cyclooxygenase-2-dependent prostaglandin synthesis in osteoblasts. J Immunol 1996;156:758-64.
PUBMED

42. Shi N, Zhang J, Chen SY. Runx2, a novel regulator for goblet cell differentiation and asthma development. FASEB J 2017;31:412-20.
PUBMED | CROSSREF

43. Baur JA, Sinclair DA. Therapeutic potential of resveratrol: the *in vivo* evidence. Nat Rev Drug Discov 2006;5:493-506.
PUBMED | CROSSREF

44. Tao K, Bai X, Jia W, Liu Y, Zhu X, Han J, et al. Effects of resveratrol on the treatment of inflammatory response induced by severe burn. Inflammation 2015;38:1273-80.
PUBMED | CROSSREF

45. Rafe T, Shawon PA, Salem L, Chowdhury NI, Kabir F, Bin Zahur SM, et al. Preventive role of Resveratrol against inflammatory cytokines and related diseases. Curr Pharm Des 2019;25:1345-71.
PUBMED | CROSSREF

46. Kim SW, Kim DW, Khalmuratova R, Kim JH, Jung MH, Chang DY, et al. Resveratrol prevents development of eosinophilic rhinosinusitis with nasal polyps in a mouse model. Allergy 2013;68:862-9.
PUBMED | CROSSREF

47. Hur DG, Khalmuratova R, Ahn SK, Ha YS, Min YG. Roles of periostin in symptom manifestation and airway remodeling in a murine model of allergic rhinitis. Allergy Asthma Immunol Res 2012;4:222-30.
PUBMED | CROSSREF

48. Shin HW, Cho K, Kim DW, Han DH, Khalmuratova R, Kim SW, et al. Hypoxia-inducible factor 1 mediates nasal polypogenesis by inducing epithelial-to-mesenchymal transition. Am J Respir Crit Care Med 2012;185:944-54.
PUBMED | CROSSREF

49. Boonrungsiman S, Gentleman E, Carzaniga R, Evans ND, McComb DW, Porter AE, et al. The role of intracellular calcium phosphate in osteoblast-mediated bone apatite formation. Proc Natl Acad Sci U S A 2012;109:14170-5.
PUBMED | CROSSREF

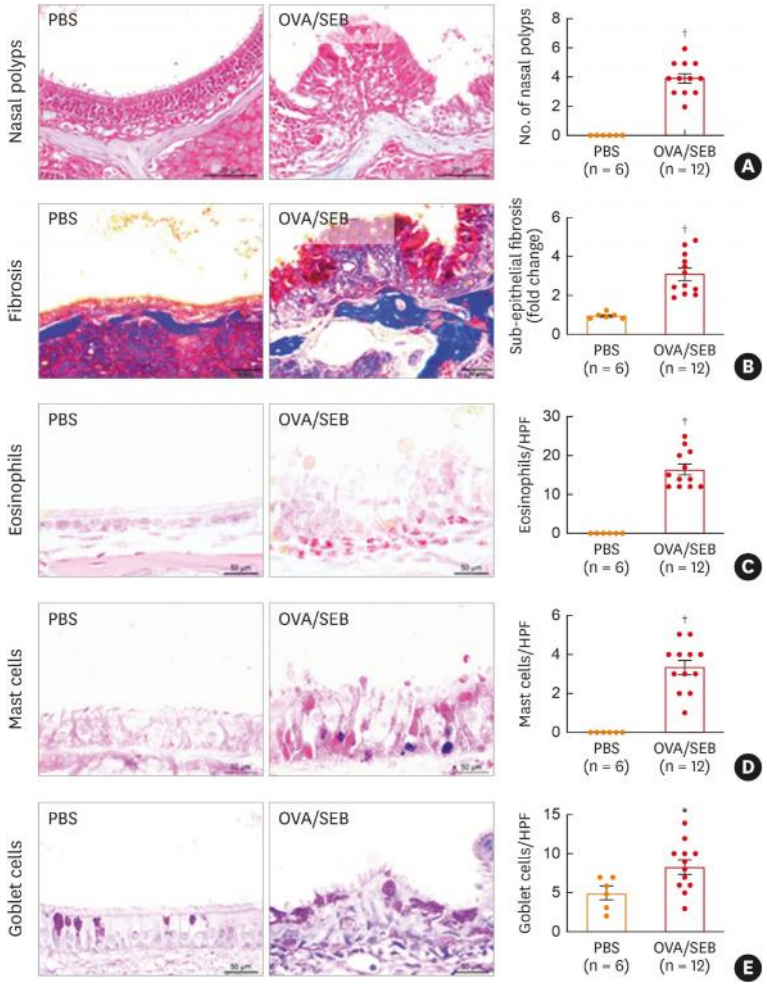

Supplementary Fig. S1. Histopathological evaluation of nasal mucosal tissue. (A) Representative H&E-stained photographs of sinonasal spaces and polyp like lesions. (B) Sub-epithelial fibrosis. (C) The number of eosinophils. (D) The number of mast cells. (E) The number of goblet cells. All results are presented as means ± SEM. Individual values are indicated by dots (A-E). Statistical significance was determined by Mann-Whitney *U* test for pairwise comparisons (A-E). Scale bars are 20 µm (A) and 50 µm (B-D).

Allergy Asthma Immunol Res. 2020 Mar;12(2):306-321.
https://doi.org/10.4168/aair.2020.12.2.306

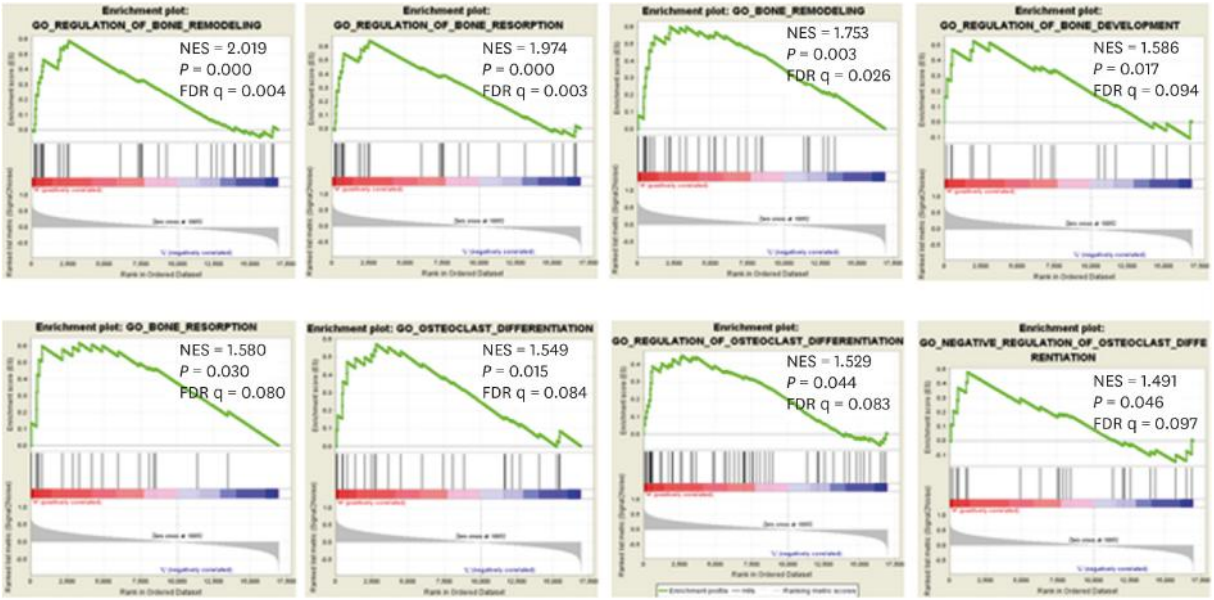

Supplementary Fig. S2. IL-13 is positively associated with high expression of osteogenesis-related gene sets. Enrichment plots of the top 8 gene sets that were positively correlated with IL-13 expression ($P < 0.05$ and FDR < 0.25).

Allergy Asthma Immunol Res. 2020 Mar;12(2):306-321.
https://doi.org/10.4168/aair.2020.12.2.306

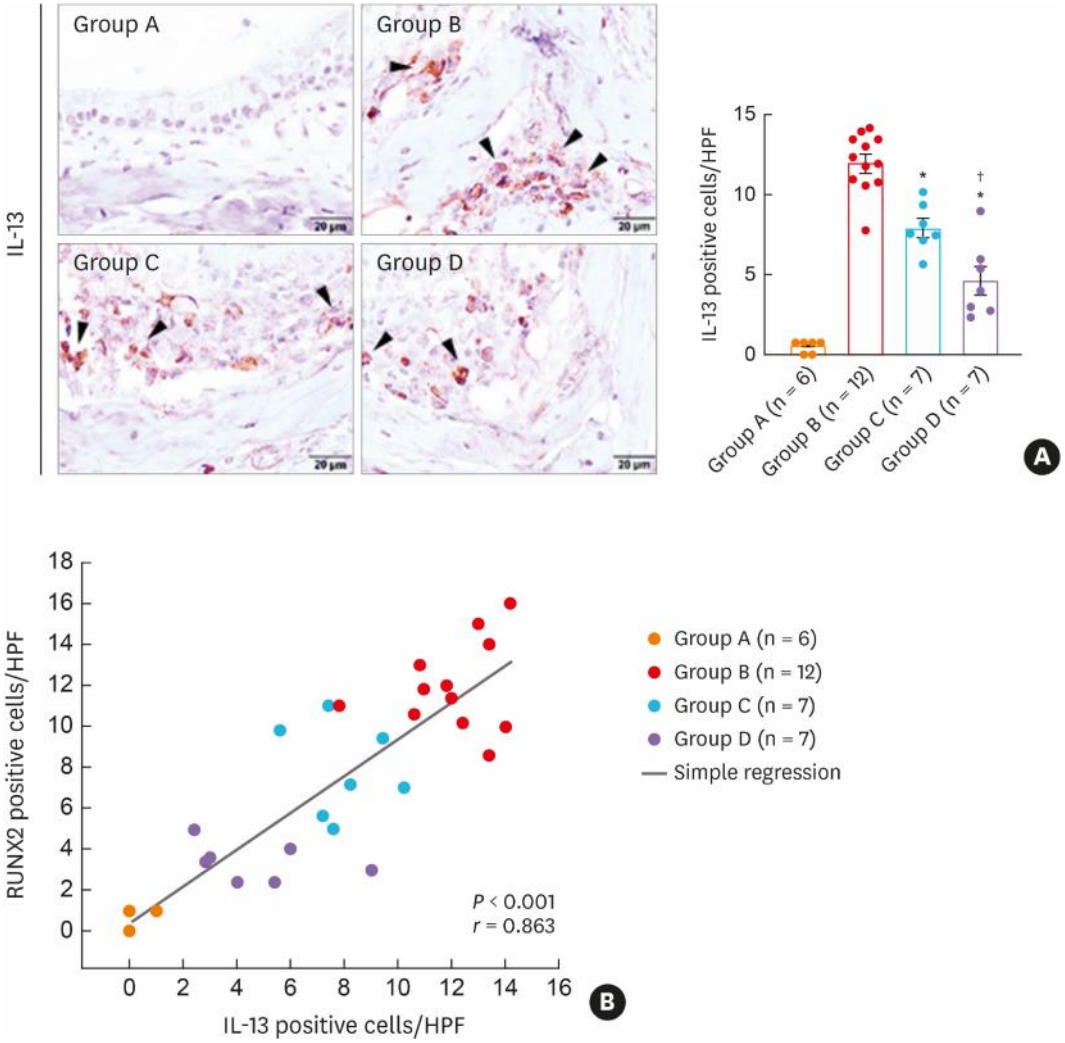

Supplementary Fig. S3. The number of IL-13 positive cells and correlation with RUNX2 positive cells. (A) The cells showing IL-13 positivity are counted per HPF were counted in indicated groups and compared (scale bar = 20 μm). (B) Relationship between IL-13 positive cells and RUNX2-positive cells. Results are presented as means ± SEM. Individual values are indicated by . . .

Allergy Asthma Immunol Res. 2020 Mar;12(2):306-321.
https://doi.org/10.4168/aair.2020.12.2.306